ACS APPLIED POLYMER MATERIALS

Open Access
This article is licensed under CC-BY 4.0

pubs.acs.org/acsapm
Article

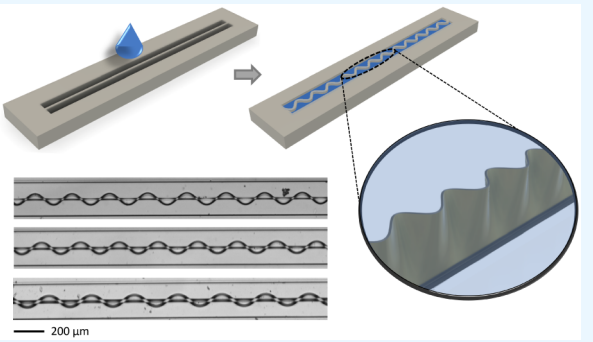
Buckling as a Tool for Spatiotemporal Sensing in Micromechanical Fluidic Systems

Abhishek Srivastava, Claas-Hendrik Stamp, Efstathios Mitropoulos, Mahdi Roshani, Andreas Greiner, Lars Pastewka, Viacheslav Slesarenko, and Thomas Pfohl*

Cite This: ACS Appl. Polym. Mater. 2026, 8, 18181−18193
Read Online

ACCESS | Metrics & More | Article Recommendations | Supporting Information

ABSTRACT: Stimulus-responsive deformations in soft materials are central to emerging strategies in microscale sensing and actuation, yet translating such behaviors into confined fluidic environments remains a challenge. Here, we introduce a microfluidic platform integrating upright polydimethylsiloxane (PDMS) membranes, which buckle predictably in response to binary isopropanol−water mixtures. Static experiments reveal that the critical buckling concentration increases with membrane thickness, while the buckling wavelength remains invariant. Finite element simulations incorporating nonlinear swelling accurately capture both the onset and amplitude of buckling. Under dynamic conditions, we observe traveling buckling waves driven by propagating solvent fronts − a phenomenon governed by the coupled kinetics of swelling, diffusion, advection, and elastic instability. These soliton-like deformations serve as self-reporting signatures of local composition gradients. Our findings establish a paradigm for solvent detection based on geometry-controlled elastic instabilities, offering a robust platform for passive, label-free chemical sensing, programmable fluidic responses, and the design of soft robotic and logic-enabled microsystems.



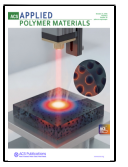
KEYWORDS: *soft membranes, swelling-induced buckling, microfluidics, elastic instabilities, solvent sensing, traveling buckling waves, stimuli-responsive materials*

INTRODUCTION

Nature ingeniously employs swelling-induced shape transformations to drive motion, sensing, and morphogenesis − from pinecones opening in response to humidity to seedpods releasing with mechanical force.[1,2] Inspired by these biological strategies, synthetic elastic membranes can exploit similar swelling-driven instabilities for programmable deformation in soft material systems. Because of their mechanical compliance, biocompatibility, and capacity for complex shape transformations under external stimuli[3,4] elastic membranes have emerged as versatile structural elements in the design of soft materials and microfluidic systems. Among these, polydimethylsiloxane (PDMS) membranes have become central to microfluidics due to their ease of fabrication, inertness, and tunable mechanical properties.[5−7] In existing literature, researchers frequently consider thin plates and membranes as interchangeable structural elements within microfluidic contexts.[8] Buckling instabilities in such membranes have attracted sustained interest across diverse applications including soft robotics,[9,10] adaptive optics,[11] mechanical sensing,[12,13] and strain-induced adhesion.[14] Buckling occurs when compressive stresses exceed a critical threshold, resulting in out-of-plane deformations that are strongly governed by geometric confinement, material properties, and external stimuli such as solvent absorption or mechanical actuation.[15−17]

Thin elastic membranes are especially prone to buckling due to their high surface-area-to-thickness ratio, making them ideal candidates for encoding programmable instabilities in soft matter systems.[18] Classical models such as Euler buckling and plate theory describe postbuckling behavior in slender structures,[19,20] while more recent work has extended these frameworks to include anisotropic materials,[21] active interfaces,[22] and nonlinear growth-induced instabilities.[23−25] Boundary conditions and confinement geometries are known to influence the resulting wrinkle morphology and wavelength selection.[26] Periodic patterns have been exploited for applications ranging from tunable optics and mechano-responsive electronics to programmable interfaces.[27−30] In particular, Stamp et al.[30] demonstrated swelling-induced buckling and hydraulic resistance modulation in high-aspect-

Received: June 11, 2026
Revised: September 29, 2026
Accepted: October 4, 2026
Published: October 13, 2026



ACS Publications
© 2026 The Authors. Published by American Chemical Society

Downloaded from pubs.acs.org/aapmcd/article-pdf/8/20/18181/6828086/acsapm.6c02520.pdf by UNIV FREIBURG user on 04 November 2026

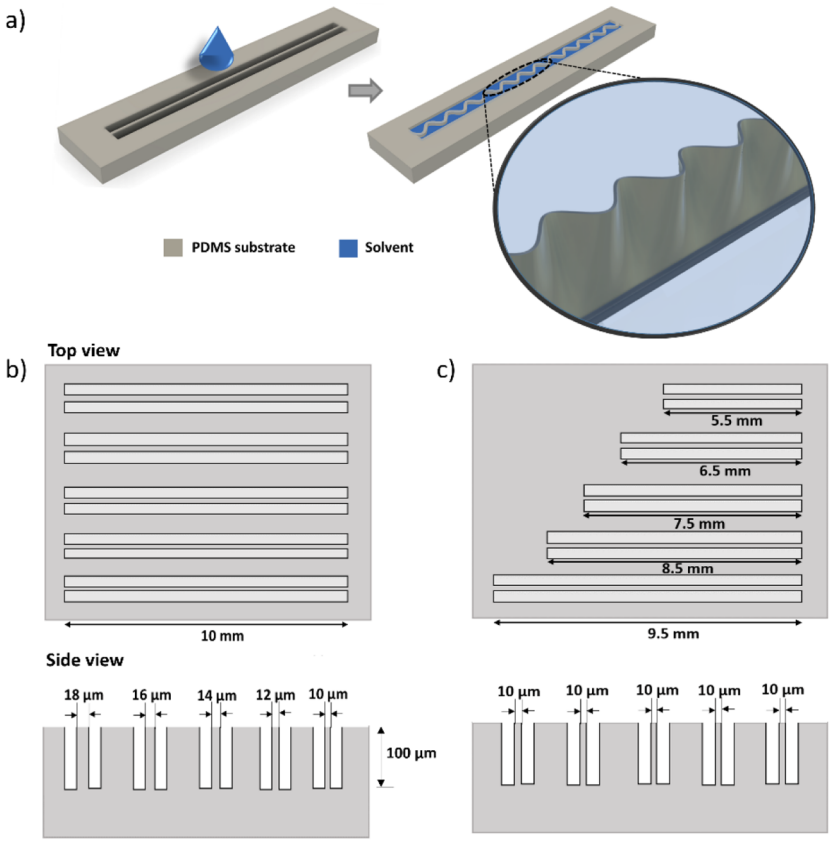


Figure 1. a) Schematic illustration of the micromechanical fluidic sensing platform. The 3D perspective view (left) shows the upright PDMS membranes embedded within a microfluidic channel and bonded at their base to the PDMS substrate. The magnified view (right) highlights the periodic sinusoidal buckling pattern of a single membrane in the presence of a swelling solvent. b) Schematic top and side views of device 1, featuring parallel membranes of a fixed length (a = 10 mm) and height (b = 100 μm) with varying membrane thicknesses (h = 10, 12, 14, 16 and 18 μm)used for static buckling characterization. c) Schematic top and side views of device 2, featuring membranes of a fixed thickness (h = 10 μm) and height (b = 100 μm) with varying channel lengths (a = 5.5 mm to 9.5 mm) used for tracking dynamic solvent fronts and traveling waves.

ratio microfluidic membranes. In contrast, the present study focuses on the transient evolution of membrane deformations under spatially and temporally varying solvent conditions.

The interaction of elastic membranes with solvents introduces a powerful platform for programmable shape change via swelling-induced mechanical instabilities. Solvent diffusion into a compliant polymer induces volumetric expansion, which under boundary confinement generates in-plane compressive stress and triggers instabilities.[31,32] The extent and kinetics of swelling are influenced by solvent diffusivity, polymer−solvent interaction parameters, and cross-linking density.[33,34] For example, instabilities in hydrogels,[35] tunable wrinkling for optics and sensing,[36−38] and mechanically guided swelling patterns[39] have all demonstrated the rich design space offered by solvent-induced deformation.

A critical determinant of buckling behavior is the membrane thickness. Thin membranes buckle at lower critical compressive loads due to reduced bending stiffness, while thicker membranes require stronger stimuli to induce instability. In wrinkling-based metrology, for example, wavelength scales with thickness and modulus.[13,40,41] In solvent-induced buckling, membrane thickness controls not only the onset threshold but also the spatial extent of deformation,[42−44] offering design principles for solvent sensing[45,46] and reconfigurable microstructures.[47]

While static wrinkling regimes have been extensively characterized, dynamic buckling remains less explored. Unlike steady-state deformations, dynamic regimes involve time-dependent evolution of mechanical instabilities under transient stimuli such as evaporation, flow, or local gradients.[48−50] These deformations can propagate as mechanical solitons or waves, and often encode real-time information about mass transport, solvent uptake, or boundary-driven instabilities.[51−55] Dynamic systems thus hold promise for autonomous sensing and computation, but require advanced understanding of fluid−structure interactions and local geometry.

Recent studies have explored various directions in this domain. Stamp et al. demonstrated that upright PDMS microstructures undergo solvent-induced buckling transitions in response to composition changes, enabling concentration sensing without the need for chemical labels.[30] Similarly, Liu et al. showed how anisotropic wrinkling can be harnessed to fabricate programmable interfaces and spatially structured polymer surfaces.[56] Furthermore, novel hydrogel-based devices that respond to solvents through directional swelling and confined motion have also been demonstrated.[57,58] Other studies have explored swelling-induced buckling in microchannels[59] and limitations in film thickness for buckling-based metrology.[60] Together, these advances reveal the potential of swelling-mediated instabilities for responsive design, real-time readout, and spatiotemporal control.

Despite these developments, the interplay between membrane geometry, solvent dynamics, and real-time buckling evolution under tight confinement remains poorly understood, particularly for upright microstructures that are embedded in

https://doi.org/10.1021/acsapm.6c02520
ACS Appl. Polym. Mater. 2026, 8, 18181−18193

Downloaded from pubs.acs.org/aapmcd/article-pdf/8/20/18181/6882086/acsapm.6c02520.pdf by UNIV FREIBURG user on 04 November 2026

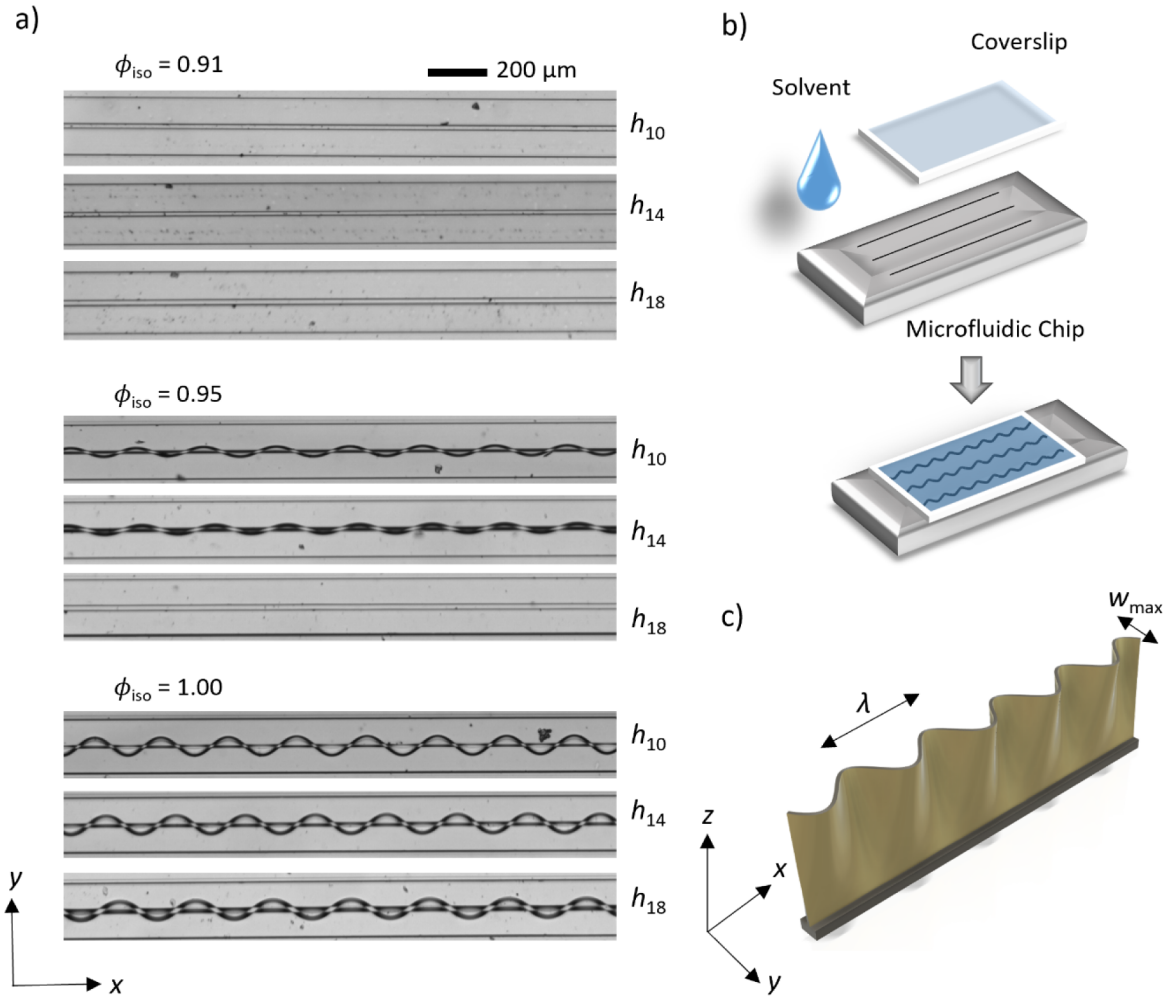


Figure 2. a) Optical microscopy images showing buckling patterns in membranes of different thicknesses (h_{10}, h_{14}, and h_{18} refer to 10 μm, 14 μm, and 18 μm, respectively) at various isopropanol concentrations, illustrating the effect of solvent concentration and membrane thickness on the buckling behavior. b) Schematic representation of the experimental setup used to induce and observe membrane buckling. c) A pseudo-3D schematic representation of the buckled membrane shape, showing a sinusoidal deformation along the membrane length.

microfluidic platforms. In this study, we investigate the static and dynamic buckling behavior of vertical PDMS membranes using binary isopropanol−water mixtures as stimuli. Our system allows us to explore how geometry and local solvent gradients influence the onset, amplitude, and spatial extent of buckling. We reveal a unique regime in which the buckling wavelength remains constant while the amplitude increases nonlinearly with solvent volume fraction − an effect captured using finite element simulations. In the dynamic regime, we observe traveling buckling waves that encode solvent motion and evaporation. By correlating membrane shape evolution with local composition, our platform enables a label-free, high-contrast readout of solvent gradients. This framework paves the way for passive sensing, spatiotemporal logic encoding, and programmable chemical actuation in soft matter systems.

MATERIALS AND METHODS

Microdevices and Optical Microscopy

The devices were fabricated using soft lithographic replica molding. The silicon master mold was prepared by Microresist (Berlin, Germany) using SU-8 photoresist and patterned by UV lithography with a 5-in. chrome photomask (Compugraphics, Jena, Germany). To prevent adhesion of PDMS during molding, the master was hydrophobized by exposure to chlorotrimethylsilane vapor (≥99%, Sigma-Aldrich, Burlington, MA, USA).

PDMS (Sylgard 184, Dow Inc., Midland, MI, USA) was mixed with curing agent at a 10:1 weight ratio by vigorous stirring and air bubbles were removed by degassing under vacuum. The degassed mixture was poured over the master and to ensure full coverage of the microstructures, a second degassing step was performed. The PDMS was then cured overnight at 65 °C. After curing, the devices were washed three times in chloroform (pa., Merck, Darmstadt, Germany) for 24 h each to remove any non-cross-linked PDMS oligomers. After washing, the devices were placed under vacuum to remove residual chloroform and to promote membrane straightening.

Two different microfluidic devices were used (Figure 1). In device 1, the membrane length was fixed at a = 10 mm, height at b = 100 μm, and thickness varied across samples: h = 10, 12, 14, 16, and 18 μm (Figure 1). In device 2, the membrane thickness was fixed at h = 10 μm, but the length varied from a = 5.5 to 9.5 mm. The membranes were upright, rectangular in cross-section, and embedded along the side walls of a microfluidic channel.

Experiments were performed using an Olympus BX61 inverted microscope equipped with an LMPlan FI 10×/0.25 objective and a DMK 33UX174 camera (Imaging Source, Germany). The device was positioned using a motorized MP-285 XYZ translation stage (Sutter Instrument Company), and image contrast and brightness were adjusted using Fiji.[61]

Downloaded from pubs.acs.org/aapmcd/article-pdf/8/20/18181/6882086/acsapm.6c02520.pdf by UNIV FREIBURG user on 04 November 2026

https://doi.org/10.1021/acsapm.6c02520
ACS Appl. Polym. Mater. 2026, 8, 18181−18193

All fluids were introduced by pipetting. Isopropanol (≥99.9%, Sigma-Aldrich) was used as the swelling solvent. In static experiments, a binary isopropanol−water mixture was prepared by volume. The isopropanol volume fraction ϕ_{iso} was defined as

$$\phi_{iso} = \frac{V_{iso}}{V_{iso} + V_{water}} \quad (1)$$

where V_{iso} and V_{water} are the volumes of isopropanol and water, respectively. The binary mixture was introduced onto the device by pipetting, fully immersing the membrane region. A thin glass coverslip (24 mm × 50 mm, thickness 0.16−0.19 mm) was gently placed over the device to minimize evaporation. A thin solvent layer, on the order of several tens of micrometers, as observed by microscopy, remained between the top edge of the membrane and the coverslip, preventing direct contact and allowing the membrane top edge to deform freely during buckling. The glass coverslip defines a quasi-two-dimensional confined geometry, ensuring a reproducible diffusion−advection environment. While minor variations in placement may slightly influence local gap height, the observed buckling dynamics is governed by robust concentration gradients and is reproducible in its qualitative spatiotemporal evolution. The buckling observed in these experiments arises directly from swelling-induced expansion of the membrane under lateral constraints.

In the dynamic experiments, the devices were first filled with pure isopropanol (ϕ_{iso} = 1.00) to induce complete membrane buckling. A droplet of water (10−15 μl, ϕ_{iso} = 0.00) was pipetted onto one edge of the coverslip. This water droplet was in direct contact with the prefilled isopropanol solution beneath the glass coverslip, displacing isopropanol, reducing local swelling and leading to progressive unbuckling. Solvent mixing occurred by a combination of diffusion and spontaneous advection beneath the coverslip. No active flow or mixing method was applied.

To induce traveling buckling waves, the devices were initially filled with a binary isopropanol-water mixture of subcritical concentration (ϕ_{iso} = 0.91), a concentration insufficient to induce buckling. A small droplet of pure isopropanol (10−15 μl, ϕ_{iso} = 1.00) was then introduced manually onto one side of the coverslip.

Finite Element Method Simulations

Finite element analysis was used to simulate the behavior of the membrane upon swelling. The simulations were performed in COMSOL Multiphysics 6.2. To match the preliminary experiments on standalone PDMS membranes, a linear elastic model with Young's modulus E = 1.5 MPa and Poisson's ratio ν = 0.495 was used to facilitate nearly incompressible behavior. To relate the isopropanol volume fraction ϕ_{iso} to the linear swelling ratio $\gamma = l/l_0$, where l and l_0 are the dimensions of the swollen and nonswollen PDMS, respectively, the following empirical relation was employed:

$$\gamma = 1 + \frac{1}{1 + \exp(-k_1(\phi_{iso} - k_2))} \quad (2)$$

The coefficients of the function, k_1 = 20.5 and k_2 = 1.12, were determined by fitting the experimental measurements reported by Stamp et al.[30] Although the presented function does not have a direct physical meaning, it accurately captures the nonlinear relationship between swelling and the concentration of isopropanol in the range of $0.92 < \phi_{iso} < 1$, which is sufficient for the simulations.

It should be noted that the model is not derived from a fully thermodynamic swelling framework and therefore does not explicitly account for polymer−solvent interaction parameters, osmotic free energy, or coupled diffusion−mechanics effects. Nevertheless, the adopted formulation accurately reproduces the experimentally observed swelling-induced deformation behavior required for the finite element analysis conducted in this work.

RESULTS AND DISCUSSION

Static Deformation of Polydimethylsiloxane (PDMS) Membranes as a Function of the Concentration of a Binary Isopropanol−Water Solution: A Method of Detecting Solvent Concentrations

For the static experiments, the vertically embedded PDMS membranes were laterally constrained and bonded to the PDMS substrate, as illustrated in Figure 1. This confinement restricts the swelling-induced expansion and generates the compressive stress responsible for membrane buckling. The surrounding bulk PDMS also undergoes solvent-induced swelling. However, its substantially larger dimensions and mechanical integration with the PDMS substrate suppress appreciable deformation compared with the thin membranes.

The static experiments and the experimental setup are illustrated in Figure 2. The membrane device was covered with a binary isopropanol-water solution and sealed with a glass coverslip in order to minimize evaporation. Once steady state swelling was reached, the membrane profiles were subjected to microscopic imaging.

Exposure to binary isopropanol-water mixtures caused the PDMS membranes to absorb solvents and swell. As the membranes were fixed laterally and bonded at the base, this expansion due to swelling was restricted and converted into in-plane compressive stress. An increase in the volume fraction of isopropanol ϕ_{iso} was observed to result in an increase of both, the degree of swelling and the resulting stress. Once the stress exceeded a critical threshold, the membranes buckled out-of-plane, forming a sinusoidal profile along their length. The transition for membranes with increasing thickness at three different isopropanol volume fractions (ϕ_{iso} = 0.91, 0.95, and 1.00) for device 1 is shown in the optical images of Figure 2a. Thinner membranes buckled at lower volume fractions of isopropanol, while thicker membranes required higher volume fractions to initiate out-of-plane deformations.

The swelling-induced strain is described by[30]

$$\varepsilon_{sw} = \left(1 + \frac{\Delta V}{V_0}\right)^{\frac{1}{3}} - 1 = \gamma(\phi_{iso}) - 1 \quad (3)$$

where $\gamma(\phi_{iso})$ is the linear swelling ratio, which depends on the isopropanol volume fraction, ΔV is the volume change due to swelling and V_0 is the volume of the nonswollen membrane.

The resulting in-plane compressive stress is given by

$$\sigma_{comp} = E \cdot \varepsilon_{sw} \quad (4)$$

To estimate the geometric dependence of the instability threshold, a simplified analytical approximation for thin elastic membranes was employed. Since $h \ll b$ in all investigated geometries, the critical buckling stress scales approximately with the square of the membrane thickness-to-height ratio. This approximation is intended to capture the dominant scaling behavior of the instability onset, whereas the finite element simulations incorporate the actual bonded boundary conditions of the experimental system. Buckling occurs when this stress exceeds the critical value

$$\sigma_{crit} = \frac{kE}{12(1 - \nu^2)}\left(\frac{h}{b}\right)^2 \quad (5)$$

where b = 100 μm is the fixed membrane height, k is a dimensionless coefficient depending on the boundary con-

Downloaded from pubs.acs.org/aapmcd/article-pdf/8/20/18181/6882086/acsapm.6c02520.pdf by UNIV FREIBURG user on 04 November 2026

https://doi.org/10.1021/acsapm.6c02520
ACS Appl. Polym. Mater. 2026, 8, 18181−18193

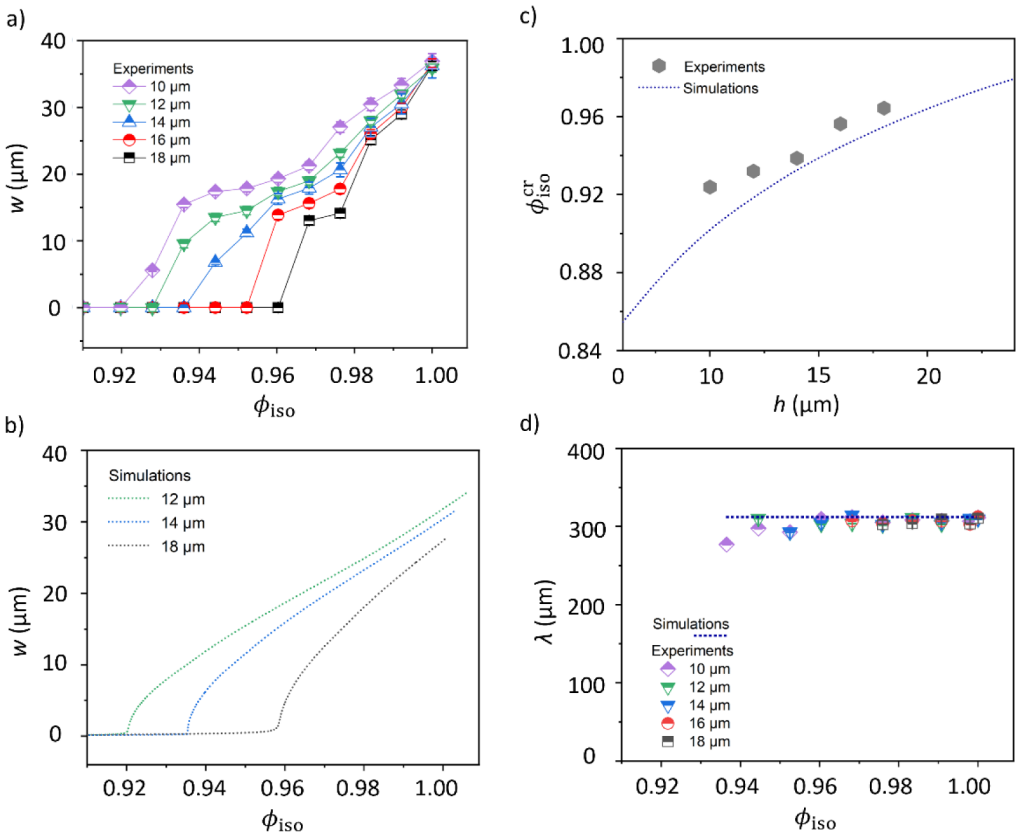


Figure 3. a) Experimentally measured buckling amplitude w as a function of ϕ_{iso} for membranes with different thicknesses h. b) Simulated buckling amplitude w for membranes of thickness h = 10, 14, 18 μm plotted against ϕ_{iso}. c) Critical buckling concentration ϕ_{iso}^{cr} as a function of h, obtained from experiments and simulations, showing strong consistency between both data sets. d) Experimental and simulated buckling wavelength λ for different ϕ_{iso} and h.

ditions and the shape of the membrane and h is the varying membrane thickness. As the critical stress scales with h^2, thinner membranes buckle more easily than thicker ones, which is consistent with the trends observed in the experiments (Figure 2a).

The buckled membrane takes on a sinusoidal shape along its free top edge, while the other three edges — the two lateral sides and the bottom — are constrained by bonding to the microfluidic channel. This lateral and vertical confinement directs the swelling-induced expansion into a periodic out-of-plane deformation characterized by a wavelength λ and amplitude w, as schematically illustrated in Figure 2c.

The critical isopropanol volume fraction ϕ_{iso}^{cr} denotes the threshold concentration above which the swelling-induced compressive stresses in the membrane exceed the buckling limit, resulting in the onset of out-of-plane deformation. Membrane deformation remains negligible for volume fractions below the critical threshold, i.e., $\phi_{iso} < \phi_{iso}^{cr}$. Once the solvent fraction exceeds this threshold ($\phi_{iso} \geq \phi_{iso}^{cr}$), the membranes undergo out-of-plane deformations, which are quantified by the amplitude w. A sharp increase in w is observed at and beyond the buckling threshold, as shown in Figure 3a. The onset of buckling occurred at different concentrations depending on membrane thickness: thinner membranes (e.g., 10 μm) buckled at a lower ϕ_{iso}, while thicker membranes required a higher isopropanol concentration to initiate deformation. This shift in the buckling threshold with respect to thickness is clearly reflected in the data presented in Figure 3a. Notably, the amplitude w remains nearly constant and close to zero below ϕ_{iso}^{cr}, followed by a rapid, nonlinear increase beyond the threshold, as shown in Figure 3a. This trend highlights the sensitivity of the membrane response to slight variations in solvent composition close to ϕ_{iso}^{cr}. The steepness of this transition is especially pronounced for thinner membranes, underscoring their potential for high-resolution detection of the solvent composition.

To complement the experiments, we ran finite element (FE) simulations to reproduce the static deformation behavior of the PDMS membranes when exposed uniformly to binary isopropanol—water mixtures. For clarity, representative finite element simulation results are shown for membrane thicknesses h = 10, 14 and 18 μm. To observe the buckling in the simulations, the concentration of the isopropanol ϕ_{iso} was gradually increased throughout the membrane volume. This procedure resulted in local swelling strains appearing according to eq 3. When ϕ_{iso} reached a critical threshold value, the membrane undergoes buckling with the formation of a sinusoidal pattern. After buckling, the amplitude of the sinusoidal patterns continued to increase with an increase of ϕ_{iso} (Figure 3b).

A comparison of Figure 3a and 3b shows that the simulations reproduce the buckling onset and the overall increase in amplitude with increasing ϕ_{iso}. However, the experimentally observed change in slope around a buckling amplitude of 15 μm is not captured by the simulations, and its physical origin remains unclear. At lower isopropanol volume fractions above the buckling threshold, the deformation amplitude shows a

https://doi.org/10.1021/acsapm.6c02520
ACS Appl. Polym. Mater. 2026, 8, 18181−18193

Downloaded from pubs.acs.org/aapmcd/article-pdf/8/20/18181/6828086/acsapm.6c02520.pdf by UNIV FREIBURG user on 04 November 2026

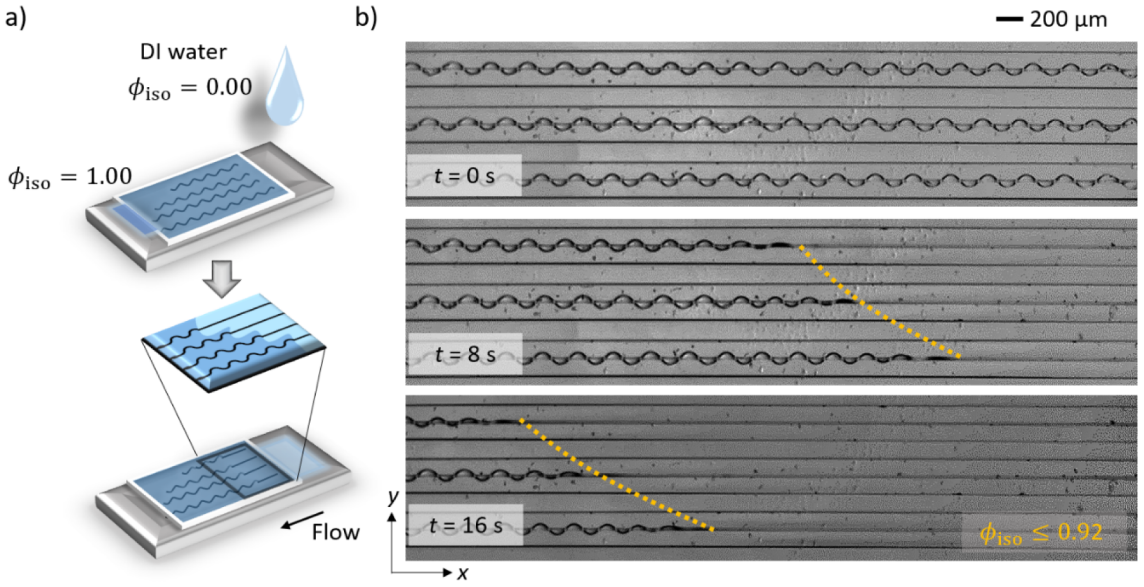


Figure 4. a) Schematic illustration of the experimental procedure used to study membrane unbuckling as an optical sensor for monitoring the evolution of a solvent concentration front in a binary solution in contact with membranes embedded in a surface. b) Time-lapse microscopic images showing the progressive unbuckling process at various times *t*. The unbuckling wavefront is clearly visible at the interface between the isopropanol and water as the front propagates across the membranes.

pronounced dependence on membrane thickness. At higher ϕ_{iso}, however, this thickness dependence becomes considerably weaker, and the experimentally observed amplitudes converge to approximately 30−35 μm. This behavior is qualitatively consistent with analytical results for swelling-induced buckling of thin strips, where the influence of the thickness-to-width ratio on the postbuckling amplitude diminishes with increasing swelling; in the thin-strip limit, the amplitude is governed predominantly by the swelling ratio and strip width.[24] Note that the linear buckling analysis, performed in addition to the simulations driven by a gradual increase in ϕ_{iso}, also showed extremely good agreement with the onset of instability. This experimentally and numerically established relationship between buckling amplitude and solvent composition provides the basis for interpreting membrane deformation in the dynamic experiments. This indicates that the linear elastic model adequately captures the onset of the buckling instability within the investigated conditions. Small differences in the precise onset point are expected because numerical simulations can detect the instability threshold immediately, whereas in experiments the onset becomes observable only after the deformation amplitude reaches optically detectable levels.

To quantitatively determine the critical isopropanol volume fraction ϕ_{iso}^{cr} required to initiate buckling, we systematically analyzed both experimental and simulation results across membranes of varying thicknesses (h = 10 to 18 μm). In the experiments, ϕ_{iso}^{cr} was identified as the mean value between the concentration at which buckling was first observed and the one at which it had not yet been observed. In the simulations, this corresponded to the swelling level at which the calculated compressive stress exceeded the critical buckling stress, as defined by eq 5. The obtained experimental and simulated values of ϕ_{iso}^{cr} for all membrane thicknesses are compared in Figure 3c. A clear trend emerges: thicker membranes require higher ϕ_{iso} values to buckle, reflecting the scaling of the critical stress with h^2.

The buckling wavelength λ is approximately 300 μm, although some deviation from this average value is observed close to the critical buckling concentration, particularly for thinner membranes (Figure 3d). At higher ϕ_{iso}, the wavelength approaches the average value and is consistent with that observed for thicker membranes. The finite element (FE) simulations show $\lambda_{sim} \approx$ 310 μm, which closely matches the experimental values. The relatively constant wavelength away from the buckling threshold indicates that λ is primarily governed by the mechanical and geometric boundary conditions, specifically, the fixed membrane height and length. It is also largely unaffected by solvent concentration for $\phi_{iso} \geq \phi_{iso}^{cr}$. Similar conclusions regarding the insensitivity of buckling wavelength to changes in concentration have been reported in previous studies of solvent-induced mechanical instabilities in polymer and hydrogel systems.[23,51]

Overall, the results demonstrate that the onset and amplitude of solvent-induced buckling in PDMS membranes can be adjusted by altering the membrane thickness. Moreover, the amplitude of buckling serves as a reliable indicator of the local ϕ_{iso}. Conversely, only low concentrations of water in the isopropanol-water binary solution are needed to prevent buckling, which can also be adjusted by varying the membrane thickness. The suppression of buckling can be directly related to the critical isopropanol volume fraction ϕ_{iso}^{cr} required to sustain the buckled state. For thinner membranes (h = 10 μm), buckling persists down to $\phi_{iso}^{cr} \approx 0.92$, corresponding to a water volume fraction of approximately $\phi_{wat} \approx 0.08$. In contrast, thicker membranes (h = 18 μm) exhibit a higher critical threshold of $\phi_{iso}^{cr} \approx 0.96$, meaning that even a small increase in water content ($\phi_{wat} \approx 0.04$) is sufficient to suppress the buckled state. This behavior reflects the thickness-dependent shift of the instability threshold rather than an intrinsic difference in sensitivity. These experimental settings provide a quantitative framework for mapping solvent concentrations in mixtures using mechanical deformations.

https://doi.org/10.1021/acsapm.6c02520
ACS Appl. Polym. Mater. 2026, 8, 18181−18193

Downloaded from pubs.acs.org/aapmcd/article-pdf/8/20/18181/6882086/acsapm.6c02520.pdf by UNIV FREIBURG user on 04 November 2026

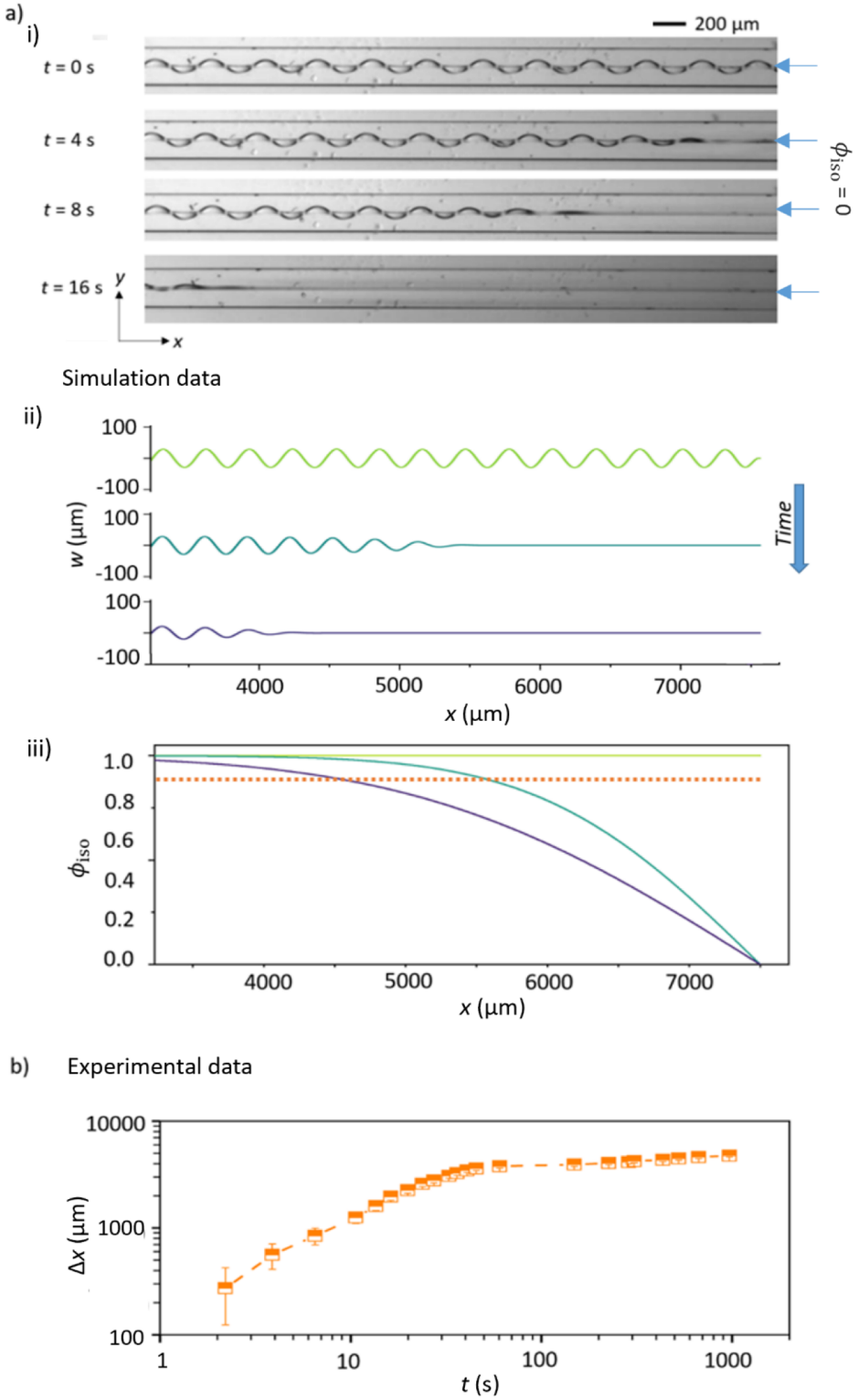


Figure 5. a) (i) Time-lapse micrographs showing the progressive unbuckling of a membrane at various t, with the unbuckled regions becoming increasingly visible over time as water replaces the isopropanol beneath the coverslip. For comparison, FE simulations of the membrane shape at three different time points: (ii) membrane deformation amplitudes w versus position and (iii) the corresponding local ϕ_{iso} profiles emulating the moving diffusive isopropanol-water interface. b) Log–log plot showing the experimentally observed position of the boundary between the buckled and unbuckled regions of the membranes, plotted as a function of time.

Downloaded from pubs.acs.org/aapmcd/article-pdf/8/20/18181/6882086/acsapm.6c02520.pdf by UNIV FREIBURG user on 04 November 2026

https://doi.org/10.1021/acsapm.6c02520
ACS Appl. Polym. Mater. 2026, 8, 18181−18193

"HydroSens": Sensing and Determination of the Water Concentration in a Binary Solution by the Unbuckling of Surface-Embedded Membranes

Because membrane buckling initiates only when the isopropanol volume fraction ϕ_{iso} exceeds a critical threshold ϕ_{iso}^{cr}, the presence or absence of localized buckling patterns enable us to judge on the local concentration of the isopropanol. We designed the microfluidic devices to exploit this feature. We used an open microfluidic device (device 2) with parallel membranes of uniform membrane thickness of h = 10 μm and varying lengths of a (Figure 1c). The device was first completely covered with pure isopropanol (ϕ_{iso} = 1.00) to induce full swelling and buckling of the membrane due to lateral constraints, as illustrated in Figure 4a. A glass coverslip was then placed over the device to prevent evaporation and establish stable reference conditions. Once the buckling was confirmed under the microscope, a small droplet of water (ϕ_{iso} = 0.00) was gently introduced to one edge of the coverslip. The water droplet formed a diffuse interface with isopropanol. It spread beneath the coverslip and gradually entered the microfluidic channels between the membranes.

Time-lapse micrographs of three parallel membranes undergoing solvent-induced unbuckling are shown in Figure 4b. These membranes were taken from larger surface areas, which are shown together with the associated movie in the Supporting Information (Supplementary video S1 and figure S1). Initially, at t = 0 s, all membranes appear fully buckled with a maximum amplitude w, corresponding to regions filled with isopropanol. At t = 8 s, the moving front of the diffuse interface formed between water and isopropanol, which was formed by dispensing the water droplet at the edge of the coverslip, is entering the field of view. The water-(rich) solution initiated partial unbuckling in the affected membrane areas, where the membranes came into contact with the water-(rich) phase. At t = 16 s, the front had moved on further, causing more sections of the membranes to become straight. The yellow dashed lines in the micrographs show the boundary between the buckled and unbuckled regions of the membranes, which indicate a local isopropanol volume fraction of $\phi_{iso} < 0.92 \approx \phi_{iso}^{cr}$ or a corresponding local water volume fraction of $\phi_{water} \gtrsim 0.08$. This unbuckling behavior is a direct result of water replacing isopropanol both in the surrounding channel and within the PDMS. This response reflects a composition-dependent swelling effect rather than selective chemical recognition of water. Due to the complete miscibility of isopropanol and water, solvent exchange occurred across a diffuse interface, resulting to a gradual decrease in ϕ_{iso}. As the swelling-induced stress locally dropped below the critical value required for buckling, the membranes transitioned progressively from a buckled to a flat state.

In the early stages, the unbuckling front advanced rapidly from the side at which the water was introduced. This regime was primarily driven by advection-enhanced exchange of isopropanol by water due to capillary effects. As the solvent interface slowed down and the concentration gradient decreased, the process transitioned to a slower regime dominated by diffusion-controlled solution transport.

To understand the unbuckling phenomenon and the shape changes of the membrane in particular, the dynamic behavior of an individual membrane is analyzed in more detail (Figure 5a). At t = 0 s, the membrane is fully buckled, exhibiting a constant maximum deflection amplitude w and a homogeneous wavelength λ along its length. For comparison, see the data for h = 10 μm and $\phi_{iso} \cong 1.00$ in Figures 2 and 3. As the moving, diffuse interphase enters the field of view of the micrographs and displaces the isopropanol-rich phase with the water-rich phase, the membrane regions near the advancing front undergo a reduction in the deformation w until they are completely flattened. Over time, the unbuckling wavefront propagates from right to left along the length of the membrane, revealing a clear correlation between the interfacial front and mechanical response of the membrane.

A quantitative analysis of the spatial positions, at which complete unbuckling of the membrane can be observed, is shown in a log−log representation in Figure 5b. The curve clearly shows two regimes. The first regime is characterized by an initial, rapid increase in distance, at which the membrane relaxes back in a straight, flattened shape. This first regime can be associated with solvent exchange and indicative of advective behavior. The second regime is slower and corresponds to a rather diffusion-controlled solvent transport and relaxation of the membrane. These results strongly suggest that the local unbuckling/buckling of the membrane is directly related to the local volume fraction ratio in the membrane, and therefore to the volume fraction ratio in the surrounding binary solution. By analyzing the dynamics of the spatial changes in membrane deformation, it is possible to determine the dominant solvent transport mechanism in the binary solution in the vicinity of the micromembranes at each stage. However, as advection and diffusion occur simultaneously and cannot be resolved independently in the present experiments, these data are not used to determine the solvent-exchange rate quantitatively.

FE simulations were performed to provide further insights and prove that unbuckling of the membranes can be attributed solely to a decrease in the local isopropanol concentration. Building on the previous study on membrane buckling, the simulations begin with a fully buckled membrane, setting ϕ_{iso} = 1.00 everywhere. Then, at the right end of the membrane, the concentration of isopropanol was set to zero, ϕ_{iso} = 0.00, triggering gradual diffusion of the water from right to left. In its turn, the resulting changes in the local ϕ_{iso} led to local unbuckling of the membrane. Note that the diffusion coefficient in simulations was chosen arbitrarily to illustrate this unbuckling, rather than capture the real advective water transport that actually occurs in the experiments. The main aim here was to correlate the obtained concentration profiles with the resulting shape of the membrane. The calculated membrane shapes at three different time points, corresponding to simulated profiles of ϕ_{iso}, are shown in Figure 5a-ii. The obtained simulation results (Figure 5a-ii) are in very good agreement with the experimental results (Figure 5a-i). As the local ϕ_{iso} decreased, the simulated membrane shape transitioned smoothly from buckled to flat (Figure 5a-iii), mirroring the behavior observed in the experiments.

The performed simulations reveal a direct, one-to-one relationship between the local volume fraction of isopropanol and the local shape of the membrane (buckled or not buckled). This relationship provides an opportunity to determine the local concentration of isopropanol simply by observing the shape of the membrane, in particular the deformation amplitude w, even when direct measurements of the concentration are not possible. Together, the results demonstrate that the shape of the membrane provides a spatially and temporally resolved readout of solvent concentration dynamics, enabling precise tracking of the local state in real time. As a possible water sensor

Downloaded from pubs.acs.org/aapmcd/article-pdf/8/20/18181/6882086/acsapm.6c02520.pdf by UNIV FREIBURG user on 04 November 2026

https://doi.org/10.1021/acsapm.6c02520
ACS Appl. Polym. Mater. 2026, 8, 18181−18193

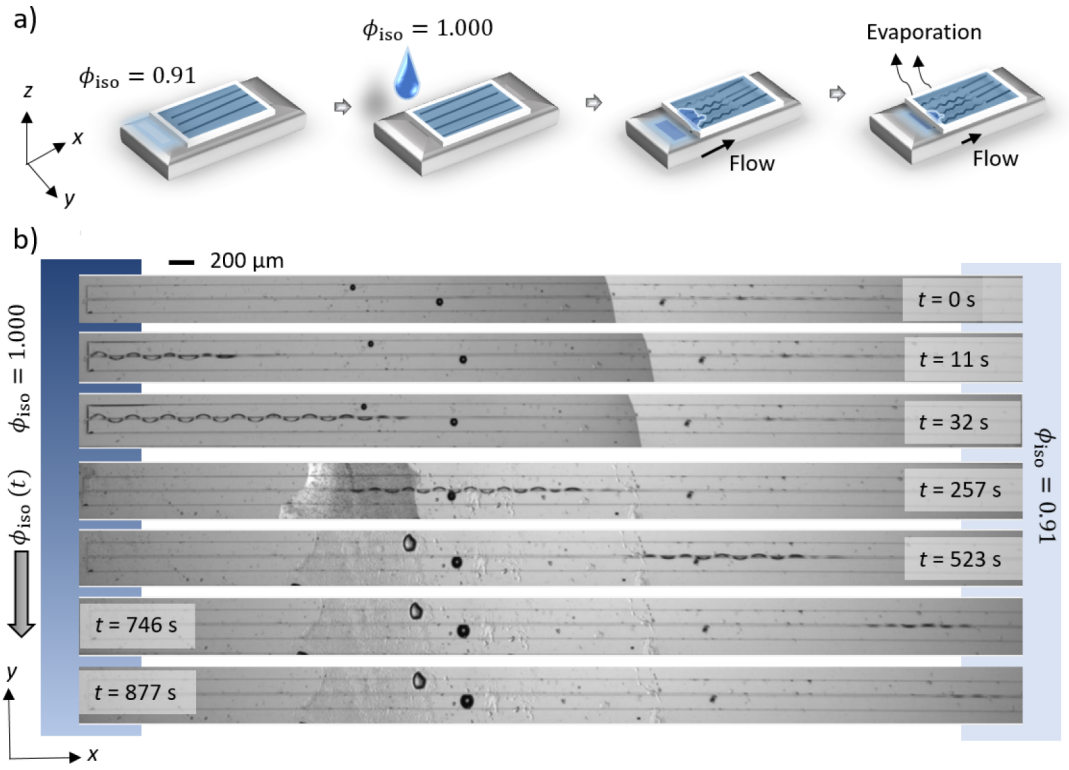


Figure 6. a) Schematic of the experimental setup and soliton wave formation after a pure isopropanol droplet (ϕ_{iso} = 1.00) is contacted with a "subcritical" isopropanol–water environment ($\phi_{iso} = 0.91 < \phi_{iso}^{cr}$). b) Time-lapse optical images showing the emergence, forward propagation, and subsequent disappearance of the traveling wave in the membrane, resulting from solvent transport and evaporation. Note: A small amount of isopropanol also spreads over parts of the top surface of the coverslip, resulting in subtle contrast variations under the microscope. Localized droplets on the glass are attributed to evaporation of isopropanol during the experiment.

("HydroSens"), the membrane response is highly sensitive to local traces of water, ϕ_{water} = 0–0.08 for device 2. The strength of the membrane buckling can be used as an optical readout, since the buckling of the membrane obviously leads to increased light scattering and a reduced transmission/reflection of the device surface. This can be visualized even at much lower optical magnifications than that used in the experiment. Depending on the chosen design, local solvent composition changes can be qualitatively or semiquantitatively inferred from the observed membrane deformation and the associated optical contrast.

Traveling Buckling Waves: "HydroSens" of the Mixing and Capillarity Behavior of Two Droplets of Binary Solutions of Different Volume Fractions

The sensitivity of the surface-embedded membranes to the volume ratio of binary solutions, particularly in the regime of low water concentrations, enabled the investigation of the complex mixing behavior of two droplets of binary isopropanol-water solutions of different volume fractions on the surface of the device. Furthermore, the interplay between capillarity and mixing resulted in the formation, evolution, and decay of a soliton-like buckling wave observed in the membranes. The dynamics is governed by the local variations in the isopropanol volume fraction (ϕ_{iso}), which are influenced by solvent transport and evaporation effects.

For these experiments, we utilized an open microfluidic device 2. The device was initially filled with a binary isopropanol–water solution at a concentration below the critical concentration at which the membrane undergoes out-of-plane deformations, $\phi_{iso} = 0.91 < \phi_{iso}^{cr}$. A thin glass coverslip was placed over the device to reduce evaporation (Figure 6a). Subsequently, a small droplet of pure isopropanol (ϕ_{iso} = 1.00) was gently dispensed onto one side of the coverslip. The solvent gradually spread underneath the glass coverslip, thereby increasing the local isopropanol volume fraction in the vicinity of the membrane. This induced a local swelling of the membrane. Due to the open geometry and the presence of drainage structures along the base of the channel, the isopropanol transport was guided by both advection and diffusion along the membrane (Figure 6b, t = 0). As the local concentration increased above the critical value $\phi_{iso}^{cr} \approx 0.92$, a localized buckled zone emerged. This initiated sinusoidal deformation propagated along the membrane, driven by the gradient in local ϕ_{iso}. The deformation zone resembled a soliton-like wave. The front of the wave is referred to the advancing buckled region and the back is referred to the initially formed, stationary buckled segment (Figure 6b, t = 11 s and 32 s). The deformation amplitude increased in regions where ϕ_{iso} exceeded ϕ_{iso}^{cr}. At the same time, the local ϕ_{iso} near the back end of the wave gradually dropped below ϕ_{iso}^{cr}, due to continuous evaporation of the dispensed isopropanol, resulting in unbuckling of the membrane in those regions. The back end of the buckled wave detached from the location of initial isopropanol dispensing and began to move forward (Figure 6b, t = 237 s). The simultaneous propagation of the front and back ends formed a traveling wave, which steadily narrowed and decreased in amplitude and length as the dispensed isopropanol continued to evaporate (Figure 6b, t = 523 s, 746 and 877 s). A time-lapse movie of a traveling membrane wave can be found in the Supporting Information (Supplementary video S2).

To analyze the traveling wave dynamics more quantitatively, the contour of the deformed membrane was tracked for different

https://doi.org/10.1021/acsapm.6c02520
ACS Appl. Polym. Mater. 2026, 8, 18181–18193

Downloaded from pubs.acs.org/aapmcd/article-pdf/8/20/18181/6828086/acsapm.6c02520.pdf by UNIV FREIBURG user on 04 November 2026

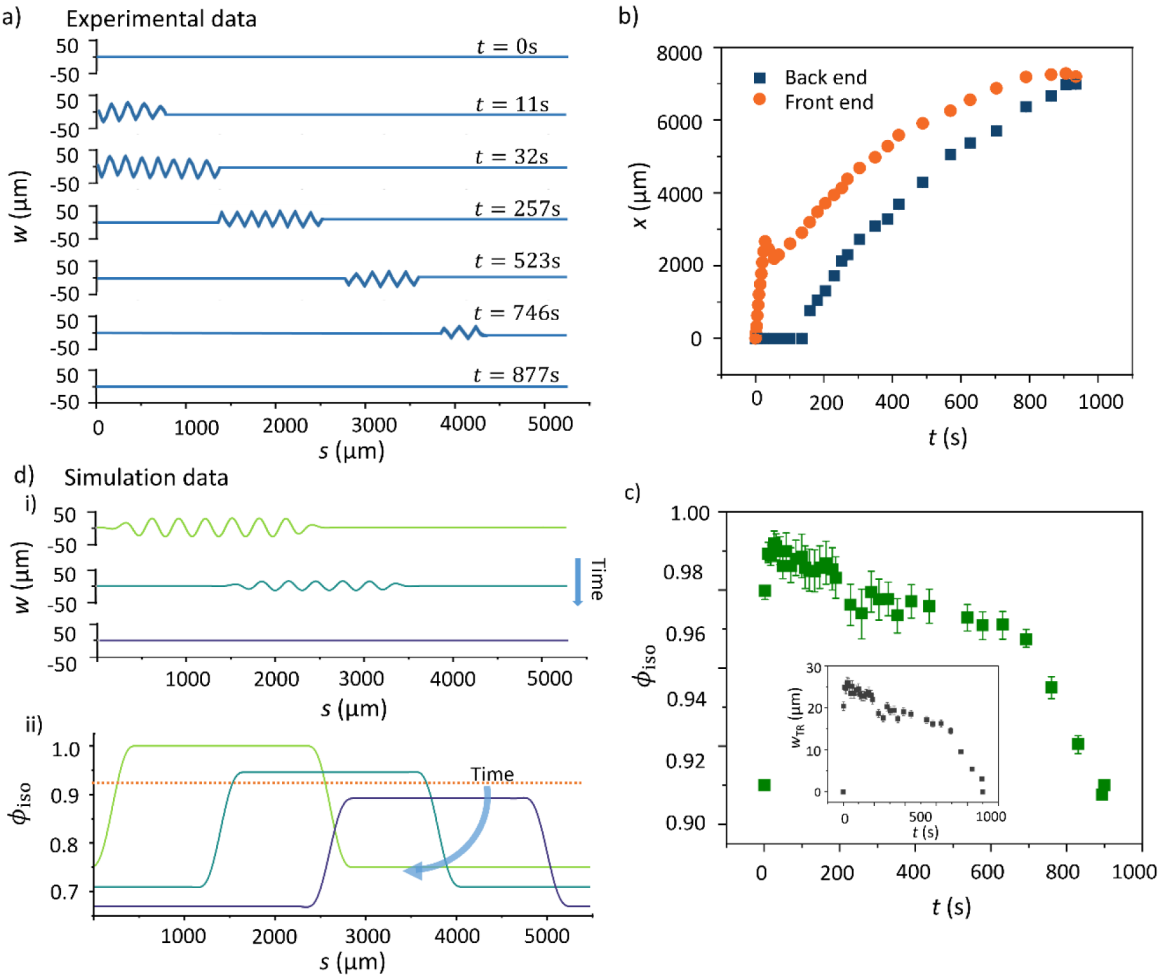


Figure 7. a) Trajectory of the length and position of the soliton buckling wave over time. b) Position of the front and back ends of the soliton buckling wave over time. c) The determined local isopropanol volume fraction ϕ_{iso} at the position of maximum buckling deformation w_{TR} as a function of time. *Inset*: w_{TR} of the moving wavefront over time. d) FE simulations of the membrane shape at three different time points: (i) membrane deformation amplitudes w versus position for the (ii) the corresponding local ϕ_{iso} profiles. (Orange dotted line represents $\phi_{iso}^{cr} = 0.92$).

time points. The obtained deformation w versus position x was plotted in Figure 7a. The positions of the front and back end of the buckling wave over time are shown in Figure 7b. Initially, buckling of the membrane was observed at the location of the membrane ($x = 0$) which was closest to the position, where pure isopropanol ($\phi_{iso} = 1.00$) was dispensed. Over time, the length of the buckled membrane increased as the front end moved forward and the back end remained fixed. At each time point, the maximum buckling deformation w_{TR} of the traveling wave was used to estimate the corresponding local ϕ_{iso} from the amplitude−concentration relationship established by the static experiments and FE simulations (Figure 3a,b). Both, w_{TR} and the corresponding ϕ_{iso}, are shown in Figure 7c. The front end of the buckling wave moved forward steadily as the solvent front propagated. However, the wavelength of the buckling wave λ_{TR} remained constant. Later, the back end of the traveling buckling wave detached and began to advance, indicating a local depletion of $\phi_{iso}(t)$ below the threshold $\phi_{iso}^{cr} = 0.92$ due to the effect of the evaporating dispensed isopropanol droplet. From this point on, the two ends of the traveling wave move in the same direction at different velocities. During this process, the maximum buckling deformations w_{TR} decreased until the traveling wave disappeared. This behavior indicates that the volume fraction of isopropanol in contact with the buckling membrane decreased during the movement of the traveling wave until it fell below the threshold, $\phi_{iso} < \phi_{iso}^{cr} \approx 0.92$.

The observation of a traveling buckling wave opens up the possibility of using previously established local concentration-shape relationships, particularly given the lack of direct access to the experimental measurements of the local isopropanol concentrations. Here, we adopt an "inverse" approach to infer the local solvent composition by analyzing the shape and evolution of the buckled membrane. Instead of starting with known concentration values and using them to predict deformation, we begin with the observed membrane deformation in simulations and work backward to estimate the isopropanol concentration that caused it (Figure 7c). This approach relies on the strong correlation between the membrane shape, which is described by the amplitude w, and the local isopropanol volume fraction ϕ_{iso}. A simulated rectangular soliton-like concentration wave moving from left to right with a constant velocity is shown in Figure 7d. This simulation recreates the traveling waves observed in the experiments. Simultaneously, the peak concentration of the isopropanol in the membrane wave gradually decreases mimicking the complex mixing and transport processes seen in the experiments. The simulated membrane shapes and the corresponding concentration wave profiles for three specific moments in time are

https://doi.org/10.1021/acsapm.6c02520
ACS Appl. Polym. Mater. 2026, 8, 18181−18193

Downloaded from pubs.acs.org/aapmcd/article-pdf/8/20/18181/6882086/acsapm.6c02520.pdf by UNIV FREIBURG user on 04 November 2026

shown in Figure 7d. As can be seen, the buckled section of the membrane moves from left to right in sync with the changes in the concentration, while the buckling amplitude gradually decreases. The membrane is completely straight when the peak concentration in the traveling wave falls below the critical value $\phi_{iso} < \phi_{iso}^{cr} \approx 0.92$. Although no real diffusion, evaporation or other physical phenomena associated with local changes of isopropanol are being directly simulated, the observed changes in the buckled shape of the membrane obtained via simulations match the experiments qualitatively and almost quantitatively. This allows us to draw conclusions about the concentration profile and its evolution in time, without the need for sophisticated − if even possible − direct experimental measurements.

This traveling wave of buckling reveals not only solvent−membrane interactions, but also demonstrates an approach to mapping local solvent compositions in microfluidic environments and on microstructured surfaces. The emergence, propagation, and dissipation of the buckled region reflect subtle gradients in the local isopropanol volume fraction, which are governed by both advection and evaporation. Although local ϕ_{iso} values were not directly measured in the experiments, the deformation profile provides an indirect, high-contrast optical readout of concentration variations, as swelling-induced buckling amplifies local solvent uptake. This behavior further suggests that arrays of such responsive microstructures could be used to visualize the evolution of concentration fronts when miscible liquids of different compositions come into contact, providing a spatial mechanical readout of mixing and solvent transport.

CONCLUSIONS

We present a solvent-responsive sensing platform based on vertically embedded PDMS membranes which undergo buckling in response to spatial and temporal variations in isopropanol−water composition. The observed response originates from swelling-induced mechanical instability of the PDMS network rather than chemically specific recognition of isopropanol. Isopropanol−water mixtures were selected here as a model system with well-characterized swelling behavior to establish the underlying sensing principles. Across three distinct experimental regimes − static, dynamic unbuckling, and traveling wave propagation − we demonstrate that membrane deformation encodes essential information about local solvent environments.

In static conditions, the onset of buckling is governed by the membrane thickness and occurs abruptly when the volume fraction of isopropanol exceeds a critical value. While the wavelength of deformation remains fixed, the amplitude increases with solvent concentration, providing a direct visual readout. Finite element simulations accurately capture this nonlinear dependence and establish a calibrated relationship between membrane deformation and solvent-induced swelling.

Dynamic experiments reveal two distinct modes of shape transformation. In the unbuckling scenario, the introduction of water displaces isopropanol beneath the membrane, which triggers the relaxation of prebuckled structures in a spatially resolved manner. In another mode, the injection of pure isopropanol into membranes that have been preconditioned with subthreshold mixtures gives rise to a traveling buckling wave. The progression and decay of this wave directly reflect transient local gradients in isopropanol concentration, revealing the remarkable sensitivity of the membrane to spatiotemporal solvent evolution.

Our approach leverages swelling-induced mechanical instabilities and embedded geometrically confined elastic elements to establish a robust, label-free strategy for local solvent sensing. The underlying principle can, in principle, be generalized to other solvent systems that produce sufficient swelling-induced stresses in PDMS or related elastomers, although the corresponding critical thresholds would depend on the specific polymer−solvent interactions. Beyond the specific isopropanol−water system investigated here, arrays of such solvent-responsive microstructures could provide a mechanically encoded means of visualizing spatial concentration gradients. For instance, when miscible droplets or liquid fronts of different compositions come into contact, spatial variations in membrane deformation could reveal the evolution of the concentration field during mixing. Such responsive surfaces could therefore provide a passive method of tracking solvent transport and mixing, while the same deformation mechanism could potentially be coupled to chemically triggered microfluidic switching.

This mechanism offers a robust alternative to electronic sensors in environments where passive, autonomous operation is required. By coupling these geometry-controlled instabilities with microfluidic logic, future implementations could enable soft logic gates that switch states based on chemical composition, or soft robotic actuators that perform sequential motion in response to a single diffusive trigger. This work thus lays the groundwork for the next generation of chemically responsive, logic-embedded soft matter.

ASSOCIATED CONTENT

Data Availability Statement

The data that support the findings of this study are available from the corresponding author upon reasonable request.

Supporting Information

The Supporting Information is available free of charge at https://pubs.acs.org/doi/10.1021/acsapm.6c02520.

Time-lapse microscopy of the water−isopropanol wavefront (Figure S1) (PDF)

Membrane unbuckling (Video S1) (MP4)

Traveling buckling-wave propagation (Video S2) (MP4)

AUTHOR INFORMATION

Corresponding Author

Thomas Pfohl − *Cluster of Excellence livMatS, FIT − Freiburg Center for Interactive Materials and Bioinspired Technologies, University of Freiburg, Freiburg 79110, Germany; Institute of Physics, University of Freiburg, Freiburg 79104, Germany;* orcid.org/0000-0002-7879-5216; Email: thomas.pfohl@physik.uni-freiburg.de

Authors

Abhishek Srivastava − *Cluster of Excellence livMatS, FIT − Freiburg Center for Interactive Materials and Bioinspired Technologies, University of Freiburg, Freiburg 79110, Germany; Department of Microsystems Engineering − IMTEK, University of Freiburg, Freiburg 79110, Germany*

Claas-Hendrik Stamp − *Cluster of Excellence livMatS, FIT − Freiburg Center for Interactive Materials and Bioinspired Technologies, University of Freiburg, Freiburg 79110,*

Downloaded from pubs.acs.org/aapmcd/article-pdf/8/20/18181/6882086/acsapm.6c02520.pdf by UNIV FREIBURG user on 04 November 2026

https://doi.org/10.1021/acsapm.6c02520
ACS Appl. Polym. Mater. 2026, 8, 18181−18193

Germany; Institute of Physics, University of Freiburg, Freiburg 79104, Germany

Efstathios Mitropoulos − *Cluster of Excellence livMatS, FIT − Freiburg Center for Interactive Materials and Bioinspired Technologies, University of Freiburg, Freiburg 79110, Germany; Institute of Physics, University of Freiburg, Freiburg 79104, Germany*

Mahdi Roshani − *Cluster of Excellence livMatS, FIT − Freiburg Center for Interactive Materials and Bioinspired Technologies, University of Freiburg, Freiburg 79110, Germany; Department of Microsystems Engineering − IMTEK, University of Freiburg, Freiburg 79110, Germany*

Andreas Greiner − *Department of Microsystems Engineering − IMTEK, University of Freiburg, Freiburg 79110, Germany*

Lars Pastewka − *Cluster of Excellence livMatS, FIT − Freiburg Center for Interactive Materials and Bioinspired Technologies, University of Freiburg, Freiburg 79110, Germany; Department of Microsystems Engineering − IMTEK, University of Freiburg, Freiburg 79110, Germany*

Viacheslav Slesarenko − *Cluster of Excellence livMatS, FIT − Freiburg Center for Interactive Materials and Bioinspired Technologies, University of Freiburg, Freiburg 79110, Germany; Department of Microsystems Engineering − IMTEK, University of Freiburg, Freiburg 79110, Germany*

Complete contact information is available at: https://pubs.acs.org/10.1021/acsapm.6c02520

Author Contributions

A.S., C.-H.S., E.M., and T.P. designed the research. A.S. and C.-H.S. performed the experiments, and V.S. performed the simulations. A.S., C.-H.S., E.M., M.R., A.G., L.P., V.S., and T.P. analyzed and discussed the data. A.S., V.S., and T.P. wrote the manuscript with the support of all authors.

Notes

The authors declare no competing financial interest.

■ ACKNOWLEDGMENTS

We would like to thank Günter Reiter and Eduardo Milana for fruitful discussions and suggestions. This work is funded by the Deutsche Forschungsgemeinschaft (DFG, German Research Foundation) under Grant No. PF375/6 within SPP 2171 and under Germany's Excellence Strategy − EXC-2193/1 − 390951807.

■ REFERENCES

(1) Reyssat, E.; Mahadevan, L. Hygromorphs: from pine cones to biomimetic bilayers. *J. R. Soc., Interface* **2009**, *6* (39), 951−957.

(2) Armon, S.; Efrati, E.; Kupferman, R.; Sharon, E. Geometry and mechanics in the opening of chiral seed pods. *Science* **2011**, *333* (6050), 1726−1730.

(3) Ionov, L. Biomimetic hydrogel-based actuating systems. *Adv. Funct. Mater.* **2013**, *23* (36), 4555−4570.

(4) Kim, J.; Hanna, J. A.; Byun, M.; Santangelo, C. D.; Hayward, R. C. Designing responsive buckled surfaces by halftone gel lithography. *Science* **2012**, *335*, 1201−1205.

(5) McDonald, J. C.; Whitesides, G. M. Poly(dimethylsiloxane) as a material for fabricating microfluidic devices. *Acc. Chem. Res.* **2002**, *35* (7), 491−499.

(6) Lee, J. N.; Park, C.; Whitesides, G. M. Solvent compatibility of poly(dimethylsiloxane)-based microfluidic devices. *Anal. Chem.* **2003**, *75* (23), 6544−6554.

(7) Brown, X. Q.; Ookawa, K.; Wong, J. Y. Evaluation of polydimethylsiloxane scaffolds with physiologically-relevant elastic moduli: interplay of substrate mechanics and surface chemistry effects on vascular smooth muscle cell response. *Biomaterials* **2005**, *26*, 3123−3129.

(8) Mitropoulos, E.; Stamp, C.-H.; Marbini, A.; Milster, S.; Dzubiella, J.; Pfohl, T. How channel elasticity enhances and directs flow in dendritic microfluidic networks. *Microsyst. Nanoeng.* **2025**, *11* (1), 254.

(9) Rus, D.; Tolley, M. T. Design, fabrication and control of soft robots. *Nature* **2015**, *521* (7553), 467−475.

(10) Kim, S.; Laschi, C.; Trimmer, B. Soft robotics: a bioinspired evolution in robotics. *Trends Biotechnol.* **2013**, *31* (5), 287−294.

(11) Shan, S.; Kang, S. H.; Wang, P.; Qu, C.; Shian, S.; Chen, E. R.; Bertoldi, K. Harnessing multiple folding mechanisms in soft periodic structures for tunable control of elastic waves. *Adv. Funct. Mater.* **2014**, *24* (31), 4935−4942.

(12) Ohzono, T.; Shimomura, M. Geometry-dependent control of instability patterns in thin elastomer films. *Phys. Rev. B* **2004**, *69*, 132202.

(13) Stafford, C. M.; Harrison, C.; Beers, K. L.; Karim, A.; Amis, E. J.; VanLandingham, M. R.; Kim, H.-C.; Volksen, W.; Miller, R. D.; Simonyi, E. E. A buckling-based metrology for measuring the elastic moduli of polymeric thin films. *Nat. Mater.* **2004**, *3* (8), 545−550.

(14) Bowden, N.; Brittain, S.; Evans, A. G.; Hutchinson, J. W.; Whitesides, G. M. Spontaneous formation of ordered structures in thin films of metals supported on an elastomeric polymer. *Nature* **1998**, *393*, 146−149.

(15) Timoshenko, S. P.; Gere, J. M. *Theory of Elastic Stability*; McGraw-Hill, 1961.

(16) Wen, T.; Ma, T.; Qian, J.; Song, Z.; Jiang, X.; Yao, Y. Phase-transition-induced dynamic surface wrinkle pattern on gradient photo-crosslinking liquid crystal elastomer. *Nat. Commun.* **2024**, *15* (1), 10821.

(17) Chung, J. Y.; Nolte, A. J.; Stafford, C. M. Surface wrinkling: a versatile platform for measuring thin-film properties. *Adv. Mater.* **2011**, *23* (3), 349−368.

(18) Huang, Z. Y.; Hong, W.; Suo, Z. Nonlinear analyses of wrinkles in a film bonded to a compliant substrate. *J. Mech. Phys. Solids* **2005**, *53*, 2101−2118.

(19) Cerda, E.; Mahadevan, L. Geometry and physics of wrinkling. *Phys. Rev. Lett.* **2003**, *90*, 074302.

(20) Efimenko, K.; Rackaitis, M.; Manias, E.; Vaziri, A.; Mahadevan, L.; Genzer, J. Nested self-similar wrinkling patterns in skins. *Nat. Mater.* **2005**, *4*, 293−297.

(21) Pezzulla, M.; Smith, G. P.; Nardinocchi, P.; Holmes, D. P. Geometry and mechanics of thin growing bilayers. *Soft Matter* **2016**, *12*, 4435−4442.

(22) Li, B.; Jia, F.; Cao, Y.-P.; Feng, X.-Q.; Gao, H. Surface wrinkling patterns on a core-shell soft sphere. *Phys. Rev. Lett.* **2011**, *106*, 234301.

(23) Mora, T.; Boudaoud, A. Buckling of swelling gels. *Eur. Phys. J. E* **2006**, *20*, 119−124.

(24) Jiang, R.; Xiao, J.; Song, J. Buckling of thin gel strip under swelling. *Theor. Appl. Mech. Lett.* **2017**, *7*, 134−137.

(25) Jin, L.; Cai, S.; Suo, Z. Creases in soft tissues generated by growth. *Europhys. Lett.* **2011**, *95*, 64002.

(26) Klein, Y.; Efrati, E.; Sharon, E. Shaping of elastic sheets by prescription of non-Euclidean metrics. *Science* **2007**, *315*, 1116−1120.

(27) Sun, J.-Y.; Xia, S.; Moon, M.-W.; Oh, K. H.; Kim, K.-S. Folding wrinkles of a thin film stiff layer on a soft substrate. *Proc. R. Soc. A* **2013**, *469*, 20120742.

(28) Tyagi, M.; Pan, J.; Jager, E. W. H. Novel fabrication of soft microactuators with morphological computing using soft lithography. *Microsyst. Nanoeng.* **2019**, *5* (1), 44.

(29) Tasoglu, S.; Diller, E.; Guven, S.; Sitti, M.; Demirci, U. Untethered micro-robotic coding of three-dimensional material composition. *Nat. Commun.* **2014**, *5*, 3124.

(30) Stamp, C.-H.; Solomon, B.; Lang, F.; Mitropoulos, E.; Pfohl, T. Tuning the hydraulic resistance by swelling-induced buckling of membranes in high-aspect-ratio microfluidic devices. *Lab Chip* **2023**, *23*, 3662−3670.

Downloaded from pubs.acs.org/aapmcd/article-pdf/8/20/18181/6882086/acsapm.6c02520.pdf by UNIV FREIBURG user on 04 November 2026

(31) Ilseng, A.; Prot, V.; Skallerud, B. H.; Stokke, B. T. Buckling initiation in layered hydrogels during transient swelling. *J. Mech. Phys. Solids* **2019**, *128*, 219−238.
(32) Ideses, Y.; Erukhimovitch, V.; Brand, R.; Jourdain, D.; Salmeron Hernandez, J.; Gabinet, U. R.; Safran, S. A.; Kruse, K.; Bernheim-Groswasser, A. Spontaneous buckling of contractile poroelastic actomyosin sheets. *Nat. Commun.* **2018**, *9* (1), 2461.
(33) Brau, F.; Damman, P.; Diamant, H.; Witten, T. A. Wrinkle to fold transition: influence of the substrate response. *Soft Matter* **2013**, *9*, 8177−8186.
(34) Stoop, N.; Lagrange, R.; Terwagne, D.; Reis, P. M.; Dunkel, J. Curvature-induced symmetry breaking determines elastic surface patterns. *Nat. Mater.* **2015**, *14* (3), 337−342.
(35) Chan, E. P.; Smith, E. J.; Hayward, R. C.; Crosby, A. J. Surface wrinkles for smart adhesion. *Adv. Mater.* **2008**, *20*, 711−716.
(36) Mei, H.; Huang, R.; Chung, J. Y.; Stafford, C. M.; Yu, H. H. Buckling modes of elastic thin films on elastic substrates. *Appl. Phys. Lett.* **2007**, *90*, 151902.
(37) Chung, S. E.; Park, W.; Shin, S.; Lee, S. A.; Kwon, S. Guided and fluidic self-assembly of microstructures using railed microfluidic channels. *Nat. Mater.* **2008**, *7*, 581−587.
(38) Kim, J.; Yoon, J.; Hayward, R. C. Dynamic display of biomolecular patterns through an elastic creasing instability of stimuli-responsive hydrogels. *Nat. Mater.* **2010**, *9*, 159−164.
(39) Zhou, Y.; Yang, L.; Liu, Z.; Sun, Y.; Huang, J.; Liu, B.; Wang, Q.; Wang, L.; Miao, Y.; Xing, M.; et al. Reversible adhesives with controlled wrinkling patterns for programmable integration and discharging. *Sci. Adv.* **2023**, *9* (15), No. eadf1043.
(40) Cai, S.; Breid, D.; Crosby, A. J.; Suo, Z.; Hutchinson, J. W. Periodic patterns and energy states of buckled films on compliant substrates. *J. Mech. Phys. Solids* **2011**, *59* (5), 1094−1114.
(41) Holmes, D. P.; Crosby, A. J. Draping films: A wrinkle to fold transition. *Phys. Rev. Lett.* **2010**, *105*, 038303.
(42) Davidovitch, B.; Schroll, R. D.; Vella, D.; Adda-Bedia, M.; Cerda, E. A. Prototypical model for tensional wrinkling in thin sheets. *Proc. Natl. Acad. Sci. U. S. A.* **2011**, *108*, 18227−18232.
(43) Genzer, J.; Groenewold, J. Soft matter with hard skin: From skin wrinkles to templating and material characterization. *Soft Matter* **2006**, *2*, 310−323.
(44) Pandey, A.; Holmes, D. P. Swelling-induced deformations: a materials-defined transition from macroscale to microscale deformations. *Soft Matter* **2013**, *9*, 5524−5528.
(45) Mirzaei, H.; McClelland, J.; Sharma, D.; Arjmand, M.; Zarifi, M. H. A microwave voyage into swelling phenomenon: investigation of polydimethylsiloxane and VOCs interaction. *ACS Appl. Mater. Interfaces* **2023**, *15*, 38008−38017.
(46) Rumens, C. V.; Ziai, M. A.; Belsey, K. E.; Batchelor, J. C.; Holder, S. J. Swelling of PDMS networks in solvent vapours; applications for passive RFID wireless sensors. *J. Mater. Chem. C* **2015**, *3*, 10091−10098.
(47) Yao, Y.; Waters, J. T.; Shneidman, A. V.; Cui, J.; Wang, X.; Mandsberg, N. K.; Li, S.; Balazs, A. C.; Aizenberg, J. Multiresponsive polymeric microstructures with encoded predetermined and self-regulated deformability. *Proc. Natl. Acad. Sci. U. S. A.* **2018**, *115*, 12950−12955.
(48) Hua, M.; Kim, C.; Du, Y.; Wu, D.; Bai, R.; He, X. Swaying gel: chemo-mechanical self-oscillation based on dynamic buckling. *Matter* **2021**, *4*, 1029−1041.
(49) Man, X.; Doi, M. Swelling dynamics of a disk-shaped gel. *Macromolecules* **2021**, *54*, 4626−4632.
(50) Imaoka, C.; Nakajima, T.; Indei, T.; Iwata, M.; Hong, W.; Marcellan, A.; Gong, J. P. Inverse mechanical-swelling coupling of a highly deformed double-network gel. *Sci. Adv.* **2023**, *9* (19), No. eabp8351.
(51) Ahmad, Z.; Tyagi, G.; Xiang, S.; Heng, J.; Patrício, P.; Teixeira, P. I. C.; Stafford, C. M.; Douglas, J. F.; Cabral, J. T. Surface wrinkling of plasma-exposed PDMS is caused by water vapor sorption: an optical environmental sensor. *Adv. Funct. Mater.* **2025**, *35*, 2509167.
(52) Li, F.; Hou, H.; Yin, J.; Jiang, X. Near-infrared light−responsive dynamic wrinkle patterns. *Sci. Adv.* **2018**, *4* (4), No. eaar5762.
(53) Metze, F. K.; Sant, S.; Meng, Z.; Klok, H. A.; Kaur, K. Swelling-activated, soft mechanochemistry in polymer materials. *Langmuir* **2023**, *39*, 3546−3557.
(54) Raney, J. R.; Nadkarni, N.; Daraio, C.; Kochmann, D. M.; Lewis, J. A.; Bertoldi, K. Stable propagation of mechanical signals in soft media using stored elastic energy. *Proc. Natl. Acad. Sci. U. S. A.* **2016**, *113*, 9722−9727.
(55) Xia, N.; Jin, D.; Pan, C.; Zhang, J.; Yang, Z.; Su, L.; Zhao, J.; Wang, L.; Zhang, J. Dynamic morphological transformations in soft architected materials via buckling instability encoded heterogeneous magnetization. *Nat. Commun.* **2022**, *13* (1), 7514.
(56) Liu, N.; Sun, Q.; Yang, Z.; Shan, L.; Wang, Z.; Li, H. Wrinkled interfaces: taking advantage of anisotropic wrinkling to periodically pattern polymer surfaces. *Adv. Sci.* **2023**, *10*, 2207210.
(57) Yao, X.; Chen, H.; Qin, H.; Wu, Q.; Cong, H.; Yu, S. Solvent-adaptive hydrogels with lamellar confinement cellular structure for programmable multimodal locomotion. *Nat. Commun.* **2024**, *15* (1), 9254.
(58) Liman, G.; Mutlutürk, E.; Demirel, G. Light- and solvent-responsive bilayer hydrogel actuators with reversible bending behaviors. *ACS Mater. Au* **2024**, *4*, 385−392.
(59) Chen, L.; Ji, D.; Sun, X.; Ding, Y.; Zhang, P.; Chen, Z.; Feng, X.; Zhu, H.; Li, Q.; Lv, W.; et al. PDMS-swelling induced microchannel reshaping and its applications in droplet microfluidics. *ACS Mater. Lett.* **2025**, *7* (6), 2172−2180.
(60) Niinivaara, E.; Desmaisons, J.; Dufresne, A.; Bras, J.; Cranston, E. D. Film thickness limits of a buckling-based method to determine mechanical properties of polymer coatings. *J. Colloid Interface Sci.* **2021**, *582*, 227−235.
(61) Schindelin, J.; Arganda-Carreras, I.; Frise, E.; Kaynig, V.; Longair, M.; Pietzsch, T.; Preibisch, S.; Rueden, C.; Saalfeld, S.; Schmid, B.; Tinevez, J. Y.; White, D. J.; Hartenstein, V.; Eliceiri, K.; Tomancak, A.; Cardona, A. Fiji: an open-source platform for biological-image analysis. *Nat. Methods* **2012**, *9*, 676−682.

Downloaded from pubs.acs.org/aapmcd/article-pdf/8/20/18181/6882086/acsapm.6c02520.pdf by UNIV FREIBURG user on 04 November 2026